PROCEEDINGS of the
23rd International Congress on Acoustics

9 to 13 September 2019 in Aachen, Germany

Determination and optimization of sound insulation capabilities of geometrically complex walls

Elias PERRAS[1]; Chuanzeng ZHANG[1]; Jihao CHEN[2]; Zhijiang JI[2]

[1] Chair of Structural Mechanics, University of Siegen, Siegen, Germany

[2] State Key Laboratory of Green Building Materials, China Building Materials Academy, Beijing, China

ABSTRACT

Several methods have been developed in the past to calculate the sound transmission in building acoustics. However, efficient determination and optimization of the sound insulation capabilities of geometrically complex walls like brick walls or layered wall structures remain a challenging task. In this work, a fully coupled fluid-structure interaction model based on the frequency-domain spectral element method (FDSEM) is proposed to determine the sound insulation characteristics of arbitrary wall structures. A virtual sound measurement laboratory following the guidelines of ISO 10140 is designed and used. The calculated frequency responses agree well with the experimental results. Therefore, this method can be used to evaluate the performance of the wall materials and structures in an efficient way. Furthermore, contrary to other methods based on the plate theory, this method is more flexible and avoids many essential simplifications, which could restrict the applicability of the methods in the wall structure design. The present method is implemented into a multi-objective optimization procedure based on a genetic algorithm to optimize various wall structures (e.g. novel brick walls, multi-functional laminates), and the results are compared with that by other numerical and analytical methods.

Keywords: Frequency-domain spectral element method, Fluid-structure interaction, Layered structures

1. INTRODUCTION

Increased energy demand and consumption, especially in developing countries, lead to the use of innovative materials and structures. These structures have to fulfill special requirements on their sound-insulation capabilities, as well as other demands such as structural and thermal properties. Experimental determination of the acoustic behavior and heat insulation property is well established, but expensive and time-consuming. Therefore, a mathematical or numerical model for predicting the insulation properties of such materials and structures is necessary to significantly reduce the costs of their design and optimization process. Numerous studies have been reported in the past for the analytical and numerical determination of the transmission loss of structures, such as sandwich panels, honeycomb panels, and double-leafed walls, e.g. (12, 20, 21). These methods can usually deliver reliable results with little computational effort, but they suffer from many restrictions which limit their validity and flexibility in analyzing structures with complex geometry. The motivation for this work is to examine the suitability and applicability of a virtual sound insulation laboratory for calculating the transmission loss of engineering structures in the design and optimization procedure. The model follows the guidelines of the ISO 10140 (9) and solves a fully coupled fluid-structure interaction (FSI) problem. To be efficient in an optimization procedure with many iterations, the required numerical calculations must be sufficiently fast. For this purpose, the problem is solved by using the spectral element method (SEM), an advanced and efficient variant of the finite element method (FEM) to increase the efficiency and accuracy of the numerical calculations.

Several authors have used a fully coupled model to determine the transmission loss of structural panels and walls. Since the computational resources necessary for the time-efficient numerical calculations at high frequencies became available only in the last two decades, most previous studies were usually only devoted to the low frequency range (5, 11). More recently, Arjunan et al. used a FEM model to determine the transmission loss of double panels (1, 2). They reported that the

[1] perras@bau.uni-siegen.de

computing time for their three-dimensional (3D) model was 30 hours by using a 2014 generation computer. Del Coz Díaz et al. used a two-dimensional (2D) model to determine the transmission loss of brick walls (6). Arjunan et al. also reported a lack of references on the use of fully coupled numerical models to determine the transmission loss of panels. Among many possible reasons for this lack is the computational effort necessary to calculate the wave propagation characteristics at high frequencies. Although the SEM is a well-established method in the meantime, no previous studies have been yet reported on a fully coupled SEM model for determining the transmission loss of wall panels used in civil engineering, to the best knowledge of the authors. Originally, the SEM was developed by Patera to solve some problems in the field of computational fluid dynamics (15), but it was also used later for a wide variety of other engineering problems such as wave propagation in functionally graded materials (7), structural health monitoring (19), seismology (10) and many others.

2. PROBLEM FORMULATION

In the determination of the transmission loss of a panel in a laboratory setting a source, usually a loudspeaker, emits a sound at varying frequencies in the source room. The resulting pressure wave excites vibrations in the panel, which in turn results again in a pressure wave in the receiving room, recorded by microphones (Figure 1, left). This process is simulated by a mathematical model. The governing equation for the fluid in the source room and the receiving room (as well as air gaps in the structure) is the Helmholtz equation for a compressible, inviscid fluid:

$$-\frac{1}{\rho}\left(\frac{\partial^2 p(\boldsymbol{x})}{\partial \boldsymbol{x}^2}+\left(\frac{\omega}{c}\right)^2 p(\boldsymbol{x})\right)=Q\,, \tag{1}$$

where ρ is the mass density of the fluid, c is the sound velocity, $p(\boldsymbol{x})$ is the spatial pressure distribution, ω is the angular frequency, and Q is the source term. To simulate a loudspeaker, a point source is used which satisfies (4)

$$\frac{\partial^2 p(\boldsymbol{x})}{\partial \boldsymbol{x}^2}+\left(\frac{\omega}{c}\right)^2 p(\boldsymbol{x})=-4\pi e^{i\varphi}\sqrt{\frac{2\rho\omega P}{4\pi^2}}\delta(\boldsymbol{x}-\boldsymbol{x}_0)\,. \tag{2}$$

where P and φ denote the power and the phase of the point source, and $\delta(\boldsymbol{x}-\boldsymbol{x}_0)$ is the Dirac-delta function. To take account of the absorption of the walls, the respective boundaries are described by an impedance Z corresponding to the reflection index r. The impedance is determined by the boundary condition:

$$\frac{1}{\rho}\boldsymbol{n}\cdot\nabla p(\boldsymbol{x})=-\frac{i\omega p(\boldsymbol{x})}{Z}\,. \tag{3}$$

In a laboratory setting, the absorption behaviour of the receiving room usually corresponds to an absorption coefficient of $\alpha \approx 0.15$. The reflection index r and the absorption coefficient α can be calculated by

$$r=\frac{Z-\rho c}{Z+\rho c} \quad \text{and} \quad \alpha=1-r^2\,. \tag{4}$$

The considered structure is described by the equations of motion for a continuum in the frequency-domain as

$$-\tilde{\nabla}^T\boldsymbol{\sigma}-\rho\omega^2\boldsymbol{u}(\boldsymbol{x})=\boldsymbol{f}\,, \tag{5}$$

where small deformation $\boldsymbol{u}(\boldsymbol{x})$ is assumed, $\tilde{\nabla}$ denotes a differential operator, $\boldsymbol{\sigma}$ is the stress tensor, ρ is the mass density of the material, and $\boldsymbol{f}$ is the body force vector. The interaction between the fluid and the structure is described by the following coupling or boundary conditions on the interface:

$$\boldsymbol{u}_S\boldsymbol{n}_F\big|_{\partial\Omega_{S,F}}=\boldsymbol{u}_F\boldsymbol{n}_F\big|_{\partial\Omega_{S,F}} \text{ and } \quad \boldsymbol{t}=-p\boldsymbol{n}_S=p\boldsymbol{n}_F \tag{6}$$

with the normal vectors $\boldsymbol{n}$ being defined in Figure 1 and the Cauchy stress vector $\boldsymbol{t}$. For further information we refer to the literature, e.g. (18).

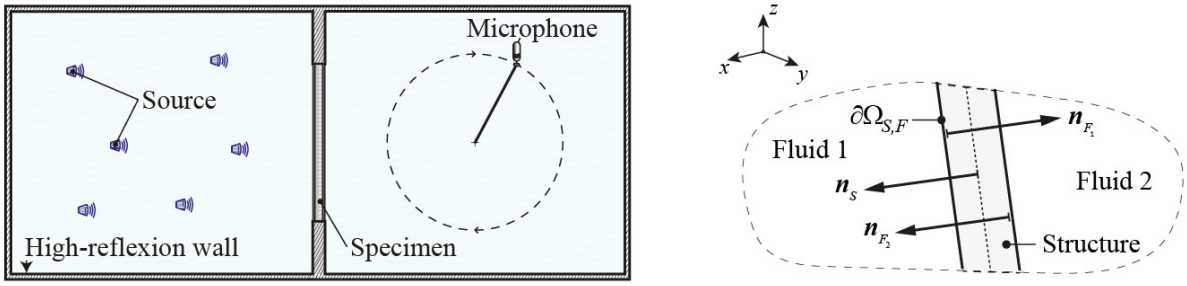

Figure 1 – Schematic representation of a virtual laboratory (left) and definition of normal vectors for the coupled fluid-structure interaction problem (right)

3. FREQUENCY-DOMAIN SPECTRAL ELEMENT METHOD

3.1 Discretization

Using the weak-form or the Galerkin method, the boundary value problem under consideration can be recast into a discretized form by approximating the pressure field with $p(\boldsymbol{x}) = \boldsymbol{N}\boldsymbol{p}$ and the displacement field with $\boldsymbol{u}(\boldsymbol{x}) = \boldsymbol{N}\boldsymbol{u}$, where $\boldsymbol{N}$ is the vector of the shape functions and $\boldsymbol{p}$ and $\boldsymbol{u}$ are the nodal pressure vector and the nodal displacement vector (17). The resulting system of algebraic equations, with neglected impedance matrix for simplicity, can be written as

$$\begin{bmatrix} \boldsymbol{K}_{F_1} - \omega^2 \boldsymbol{M}_{F_1} & -\rho_{F_1}\omega^2 \boldsymbol{C}_1^T & 0 \\ \boldsymbol{C}_1 & \boldsymbol{K}_S - \omega^2 \boldsymbol{M}_S & -\boldsymbol{C}_2 \\ 0 & \rho_{F_2}\omega^2 \boldsymbol{C}_2^T & \boldsymbol{K}_{F_2} - \omega^2 \boldsymbol{M}_{F_2} \end{bmatrix} \begin{bmatrix} \boldsymbol{p}_1 \\ \boldsymbol{u} \\ \boldsymbol{p}_2 \end{bmatrix} = \begin{bmatrix} \boldsymbol{Q}_1 \\ \boldsymbol{f} \\ \boldsymbol{Q}_2 \end{bmatrix}, \tag{7}$$

where $\boldsymbol{K}$ and $\boldsymbol{M}$ denote the system stiffness matrices and mass matrices for the fluid domain (denoted by F) and the structural domain (denoted by S) respectively, and $\boldsymbol{C}$ is the coupling matrix (18).

3.2 Basics of the Spectral Element Method

The shape functions used in the developed SEM algorithm are the Lagrange polynomials LA_p for the interpolation order p given by:

$$LA_{p,\beta}(\xi) = \prod_{\substack{\alpha=1 \\ \alpha\neq\beta}}^{p+1} \frac{\xi - \xi_\alpha}{\xi_\beta - \xi_\alpha} \tag{8}$$

which are constructed by using the nodal set ξ_i.

If evenly distributed nodes over the interval $[0;1] := \{\xi \epsilon \mathbb{R} | 0 \le \xi \le 1\}$ are chosen, strong oscillations with high orders occur, which is the so-called Runge-effect. This can be avoided by using the zeros of the Lobatto polynomial $LO_{p\text{-}1}$ as the locations for inner nodes to construct the Lagrange polynomials or the GLL nodal set. The Lobatto polynomials can be calculated by

$$LO_n(\xi) = \frac{\mathrm{d}L_{n+1}(\xi)}{\mathrm{d}\xi} \quad \text{with} \quad L_n(\xi) = \sum_{k=0}^{\lfloor n/2 \rfloor} (-1)^k \frac{(2n-2k)!}{(n-2k)!(n-k)!k!2^n} \xi^{n-2k}. \tag{9}$$

By using the GLL shape functions, some numerical difficulties can be overcome since the condition number of the coefficient matrix in Eq. (7) is much lower and allows us to use higher-order shape functions. This, in turn, leads to a spectral convergence of the method, hence the name spectral element method. It also offers the possibility of using the Lobatto quadrature for the numerical calculation of the element mass matrices (17).

Figure 2 shows the set of the shape functions of a polynomial order $p = 8$ for an evenly distributed nodal set and a GLL nodal set. The nodal set ξ_i is shown as red dots.

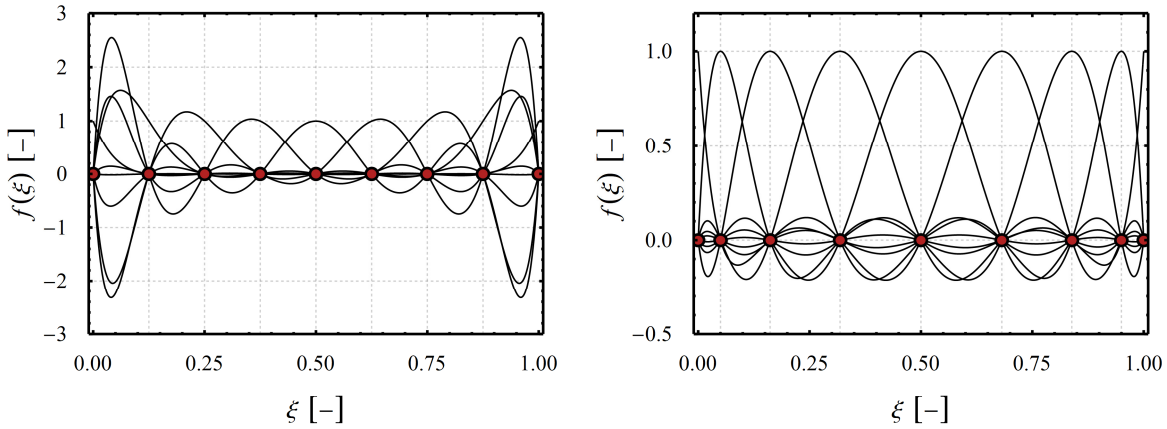

Figure 2 – Shape functions with evenly distributed nodes (left) and GLL distribution (right)

3.3 Advantages of using SEM for FSI Problems

One major advantage of the SEM is the reduced number of the degrees of freedoms (DOFs) necessary to achieve a given error threshold. Here, a one-dimensional (1D) model problem is used for demonstrating this advantage. The model is also used to a priori estimate the necessary order p and element size for a given error threshold (3). The governing equation and boundary conditions (BCs) are given by

$$\begin{gathered} \Delta p(x) + k^2 p(x) = 0\,, \quad x \in [0;L]\,, \\ \text{BCs:}\ \ \nabla p(0)\cdot n + ikp(0) = 1 \ \ \text{and} \ \ \nabla p(L)\cdot n + ikp(L) = 0\,, \end{gathered} \tag{10}$$

where $k = \omega/c$ is the wave number, and n is the outward normal vector of the boundary. The error can be calculated by using the analytical solution for the problem $p(x,k) = -(ie^{ikx})/(2k)$. The error ϵ_2 is defined as

$$\epsilon_2 = 100 \cdot \sqrt{\sum_{n=1}^{N} \left(p_n^{SEM} - p_n^{ref}\right)^2} \Big/ \sqrt{\sum_{n=1}^{N} \left(p_n^{ref}\right)^2} \tag{11}$$

with p^{ref} being the analytical solution. The boundary value problem described by Eq. (10) is solved using the SEM. By varying the number of DOFs per wavelength for a given interpolation order p we can obtain Figure 3, from which the following conclusions can be drawn:

- For a low error threshold, such as $\epsilon_2 = 0.05\%$, the necessary number of nodes per wavelength decreases significantly with increasing order. For lower error thresholds, which are not shown in the figure, the effect is even more pronounced.
- For a high error threshold, the use of higher order p gives rise to less advantages.

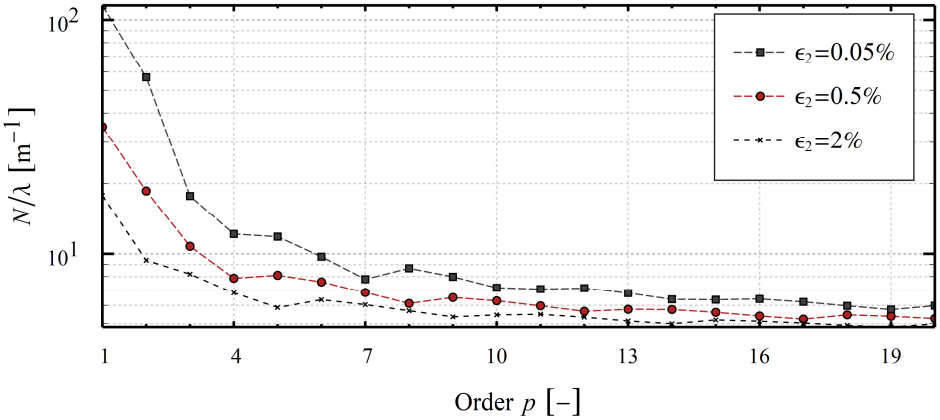

Figure 3 – Number of nodes per wavelength N/λ needed to satisfy a given error threshold ϵ_2

Since the computational effort for calculating the element matrices increases significantly, the highest order used for achieving a low error threshold should be $p = 10$ to avoid overcompensation. However, for calculating a large number of frequencies the element matrices do not need to be evaluated repeatedly, therefore the most time-consuming part usually is the solution of the linear

system of equations. In Figure 4, the number of DOFs and the time for solving the linear system of equations t_{LS} using the direct solver PARDISO (16) are shown.

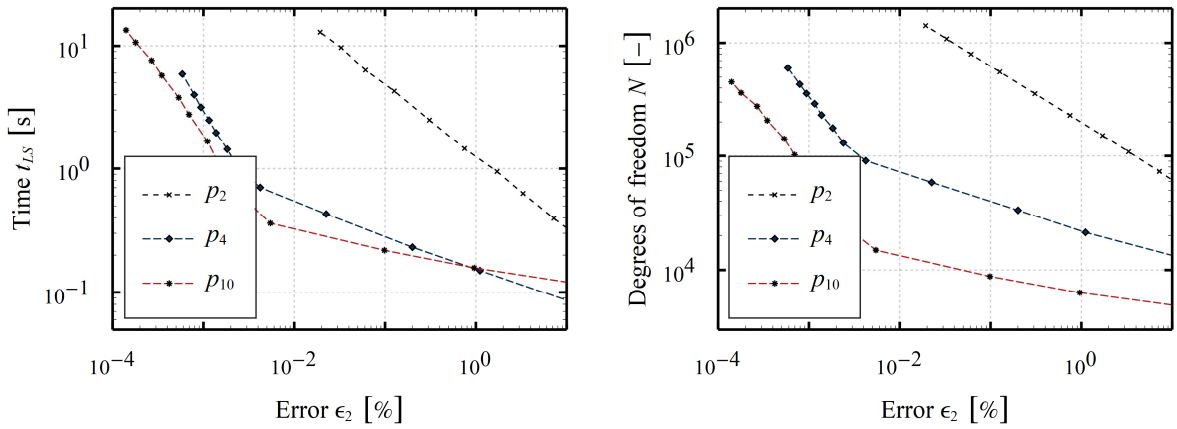

Figure 4 – Comparison of the DOFs (left) and solution time (right)

After evaluating the pressure field in the source room and the receiving room by solving Eq. (7), the sound reduction index can be calculated by

$$R = 20\lg\frac{p_l}{p_0} - 20\lg\frac{p_r}{p_0} + 10\lg\frac{S}{A_e} \tag{12}$$

with the sound pressure p_l in the source room and p_r in the receiving room, $p_0 = 20 \cdot 10^{-6}$ Pa, the area of the specimen S and the equivalent absorption area A_e (14). Eq. (12) is evaluated for a high number of frequencies for every 1/3 octave between 100 Hz and 3150 Hz. To assess the speed of the developed algorithm, a comparison with the commercial FEM software COMSOL Multiphysics 5.3 (4) was done using a layered panel and the 1D error estimator (Figure 3) to determine the necessary meshing resolution. The results are shown in Figure 5, in which the time t_{tot} for the calculation of the transmission loss curve is given. Only for a low error threshold, such as $\epsilon_2 = 0.001\%$, the advantage of the SEM using high order shape functions can be clearly observed. The efficiency increases for higher frequencies (higher number of DOFs) and lower error threshold. The reasons for the algorithm being faster than the commercial software for a high error threshold could be:

- Pre-calculation and storage of the data for the fluid domains, since they have to be calculated only once and can be reused for further calculations.
- Computation of the element mass matrices using the Lobatto integration introduces a negligible error but significantly reduces the number of the matrix operations for the assembly process for each frequency. The time-saving effect here is larger than expected.
- For high orders of the shape functions and high frequencies the parallelized calculation of several frequencies instead of the parallelized solution of the linear system of equations is more time-efficient and was used where appropriate.
- Use of different orders of the shape functions in different directions for thin elements reduces the number of DOFs for the considered structure (8).

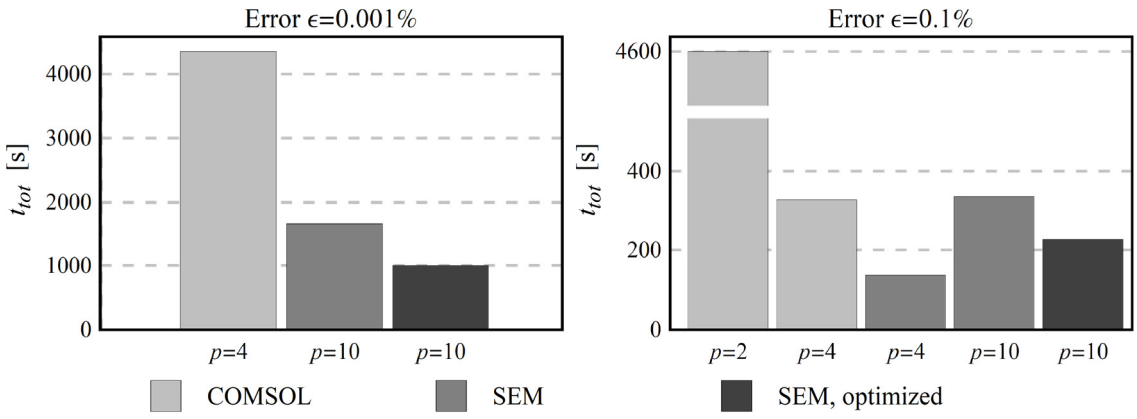

Figure 5 – Comparison of COMSOL and SEM for different orders p

Figure 6 shows a good agreement between the predicted and the measured sound reduction index R for an aluminum plate. For the layered wall, the deviations are rather large. The reasons could be uncertainties in the material properties and mainly due to lacking knowledge about the measurement conditions including the exact size of the laboratory, the absorption properties and the mounting conditions of the specimen. The latter problem occurs not only in a virtual laboratory but also in the experimental determination of R. Meier et al. found in their inter-laboratory-test that the deviations for the same specimen could be of up to 20 dB in the low frequency range and 4-8 dB in the mid and high frequency range (13).

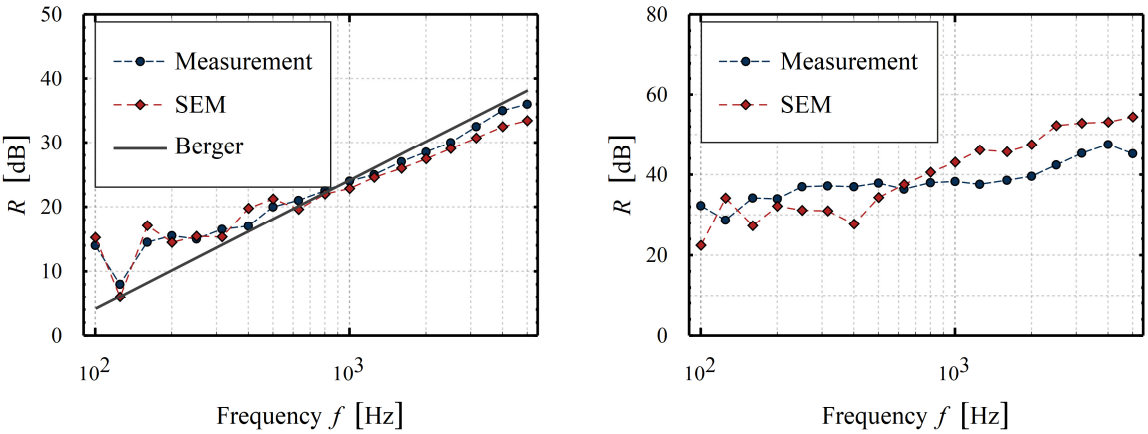

Figure 6 – Comparison between the measurement (data from Villot et al. (21)) and calculation results by the SEM and Berger's mass law (14) of a thin aluminum plate (left), and comparison between the measurement (data from CBMA) and calculation results for a layered panel (see Figure 7)

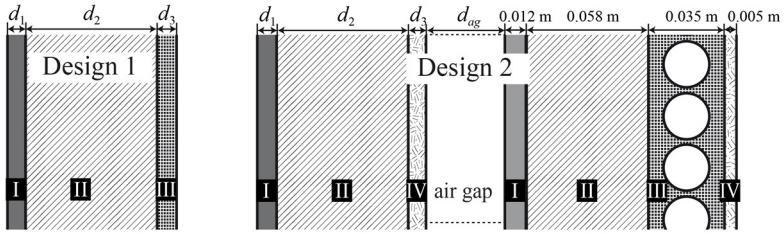

		E	ρ
I	Concrete	25	2300
II	Compressed straw panel	2.4	475
III	Shaving board	2.9	650
IV	Calcium silicate panel	3.75	1270

Figure 7 – Examples of some examined complex layered structures, E is Young's modulus in [GPa], ρ is the mass density in [kg/m^3]

4. OPTIMIZATION SCHEME

An integer value for the sound insulation capabilities can be calculated using a procedure described in the ISO 717 (14). Since an optimization algorithm requires a rather smooth function, the procedure was adjusted by using a smaller step-size to obtain a single value R_w with several decimals. This provides a smooth curve of $R_w(d_i)$, such as shown in Figs. 8 and 9, instead of the discontinuous staircase function when the ISO 717 is directly applied.

The eigenfrequencies of the laboratory and the specimen have a significant effect on the transmission loss curve. To assess the necessary number of frequencies per 1/3 octave n_t and the necessary accuracy, a test specimen with a varying thickness d_{wall} was examined (Figure 8). The necessary error threshold was found to be ϵ_2<1% and the number of frequencies per 1/3 octave should be n_t>20.

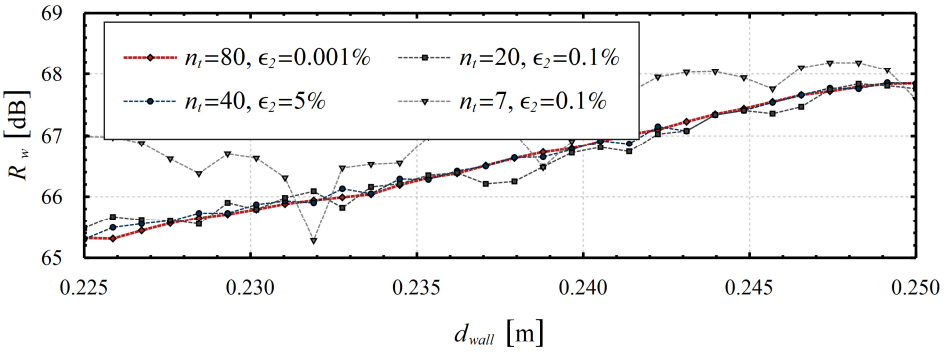

Figure 8 – Effects of the error threshold ϵ_2 and the number of frequencies per 1/3 octave n_t

The designs 1 and 2 as shown in Figure 7 were optimized regarding their acoustic insulation capabilities. The objective function and constraints are defined by

$$F_{\text{Design 1}} = \max R_w\left(d_1, d_3\right),\ F_{\text{Design 2}} = \max R_w\left(d_2, d_{ag}\right)$$

$$\text{subject to} \quad \begin{array}{ll} \sum d_i = 0.07,\ 0.005 \le d_1 \le 0.04,\ 0.002 \le d_3 \le 0.04 & \text{design 1} \\ \sum d_i = 0.26,\ 0.005 \le d_2 \le 0.06,\ 0.0025 \le d_{ag} \le 0.08,\ d_1 = d_3 & \text{design 2} \end{array} . \tag{13}$$

The numerical calculations of the objective function for a high number of functional values require a large computational effort. For a large search space, an evolutionary algorithm can be used. It is possible to find a good solution for Eq. (13) in less than 100 iterations respectively, which require a few hours for the optimization procedure. For the sake of brevity, more details, however, are not presented here.

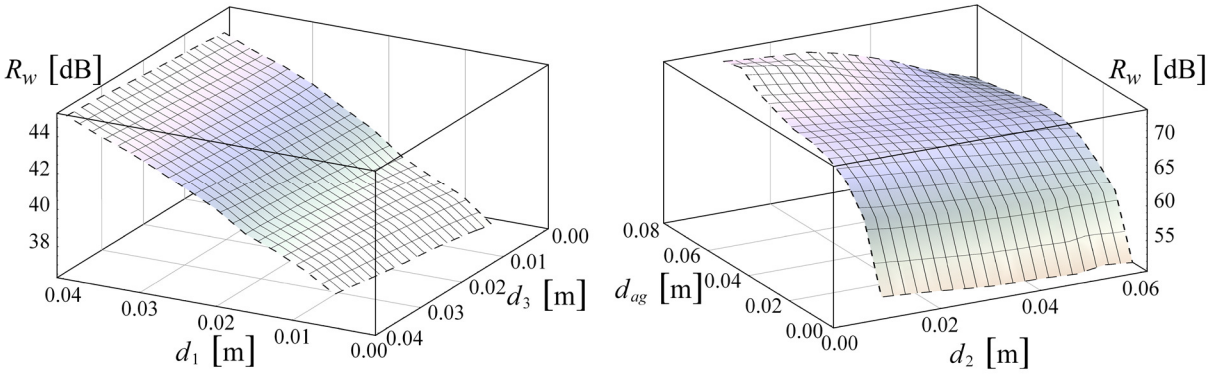

Figure 9 – Objective function for Design 1 (left) and Design 2 (right)

5. CONCLUSIONS

In this paper, a SEM in the frequency-domain is presented for calculating the transmission loss of layered wall structures by using a virtual laboratory and a fully coupled model for considering the fluid-structure interaction. For high frequencies and high accuracy, the SEM is an efficient method to evaluate the acoustic pressure field in the fluid and the structural deformations. However, for comparison with many experimental measurements, the calculation of the sound reduction index with a low accuracy is usually sufficient, diminishing some of the advantages of the SEM. For an optimization algorithm, the objective function should be evaluated with higher accuracy, regarding the error threshold of the calculation and the number of frequencies, to avoid random oscillations of the transmission loss curve. The developed SEM algorithm here reduces the time required for the numerical evaluation by up to 80% for layered wall structures. This allows for a higher number of iterations and therefore for a larger search space.

The efficiency of the algorithm decreases for a geometrically complex structure, such as Design 2 (Figure 7). To approximate the complex geometry a high number of small elements is needed. The order of the shape functions is taken as identical for both the fluid and the structural domains and therefore unnecessary DOFs are introduced, since the requirement for a given error threshold is already fulfilled by much larger elements. This problem can be avoided by using different orders for

the shape functions for the fluid and the structural domains, which require special coupling algorithms. This is a part of our further research.

ACKNOWLEDGEMENTS

This work was partially supported by the International Science & Technology Cooperation Program of China (2014DFA71290). The experimental data have been provided by the China Building Materials Academy, Beijing, People's Republic of China.

REFERENCES

1. Arjunan A, Wang CJ, Yahiaoui K, Mynors DJ, Morgan T, Nguyen B, et al. Development of a 3D finite element acoustic model to predict the sound reduction index of stud based double-leaf walls. Journal of Sound and Vibration. 2014;333:6140–6155.
2. Arjunan A, Wang CJ, Yahiaoui K, Mynors DJ, Morgan T, English M. Finite element acoustic analysis of a steel stud based double-leaf wall. Building and Environment. 2013;67:202–10.
3. Beriot H, Prinn A, Gabard G. Efficient implementation of high-order finite elements for Helmholtz problems. International Journal for Numerical Methods in Engineering. 2016;106:213–240.
4. Comsol Inc. COMSOL Multiphysics Reference Manual 5.3. Comsol Multiphysics; 2018.
5. Davidsson P, Brunskog J, Wernberg P-A, Sandberg G, Hammer P. Analysis of sound transmission loss of double-leaf walls in the low-frequency range using the finite element method. Building Acoustics. 2004;11(4):239–57.
6. Del Coz Díaz JJ, Rabanal FPÁ, Nieto PJG, López MAS. Sound transmission loss analysis through a multilayer lightweight concrete hollow brick wall by FEM and experimental validation. Building and Environment. 2010;45(11):2373–86.
7. Hedayatrasa S, Bui TQ, Zhang C, Lim CW. Numerical modeling of wave propagation in functionally graded materials using time-domain spectral Chebyshev elements. Journal of Computational Physics. 2014;258:381–404.
8. Hennings B, Lammering R, Gabbert U. Numerical simulation of wave propagation using spectral finite elements. CEAS Aeronautical Journal. 2013;4:3-10.
9. ISO 10140-5. Akustik –Messung der Schalldämmung von Bauteilen im Prüfstand –Teil 5: Anforderungen an Prüfstände und Prüfeinrichtungen. Germany; 2014.
10. Komatitsch D, Liu Q, Tromp J, Süss P, Stidham C, Shaw JH. Simulations of ground motion in the Los Angeles basin based upon the spectral-element method. Bulletin of The Seismological Society of America. 2004;94:187–206.
11. Maluski SPS, Gibbs BM. Application of a finite-element model to low-frequency sound insulation in dwellings. The Journal of the Acoustical Society of America. 2000;108(4):1741–51.
12. Mechel F. Formulas of Acoustics. Berlin: Springer-Verlag; 2008.
13. Meier A, Schmitz A, Raabe G. Inter-laboratory test of sound insulation measurements on heavy walls: Part II - Results of main test. Building Acoustics. 1999;6(3):171–86.
14. Möser M. Technische Akustik. 9.,aktualisierte Auflage. Berlin: Springer-Verlag; 2012.
15. Patera AT. A spectral element method for fluid dynamics: Laminar flow in a channel expansion. Journal of Computational Physics. 1984;54(3):468–88.
16. Petra C, Schenk O, Lubin M, Gäertner K. An augmented incomplete factorization approach for computing the Schur complement in stochastic optimization. SIAM Journal on Scientific Computing. 2014;36(2):C139-C162.
17. Pozrikidis C. Introduction to Finite and Spectral Element Methods Using MATLAB. Second Edition. Boca Raton: CRC Press, Taylor & Francis Group; 2014.
18. Sandberg G, Wernberg P-A, Davidsson P. Fundamentals of Fluid-Structure Interaction. CISM International Centre for Mechanical Sciences, Courses and Lectures. 2009. p. 23–101.
19. Schulte RT. Modellierung und Simulation von wellenbasierten Structural Health Monitoring - Systemen mit der Spektral-Elemente Methode. University of Siegen; 2010.
20. Tadeu A, António J, Mateus D. Sound insulation provided by single and double panel walls - A comparison of analytical solutions versus experimental results. Applied Acoustics. 2004;65(1):15–29.
21. Villot M, Guigou C, Gagliardini L. Predicting the acoustical radiation of finite size multi-layered structures by applying spatial windowing on infinite structures. Journal of Sound and Vibration. 2001;245(3):433–55.